International Journal of Precision Engineering and Manufacturing, Vol. 5, No. 2, April 2004.

Corrective Machining Algorithm for Improving the Motion Accuracy of Hydrostatic Bearing Tables

Chun Hong Park[1,#], Chan Hong Lee[1] and Husang Lee[1]

[1] Machine tools group, Korea Institute of Machinery & Materials, Daejeon, South Korea

ABSTRACT

For improving the motion accuracy of hydrostatic tables, a corrective machining algorithm is proposed in this paper. The algorithm consists of three main processes. The reverse analysis is performed firstly to estimate the rail profile from the measured linear and angular motion error, in the algorithm. For the next step, the corrective machining information is obtained based upon the estimated rail profile. Finally, the motion errors on the correctively machined rail are analyzed by using the motion error analysis method. These processes are iterated until the analyzed motion errors are satisfactory within the target accuracy. In order to verify the validity of the algorithm theoretically, the motion errors calculated by the estimated rail after the corrective machining process, are compared with those by the true rail which is previously assumed as the initially measured value. The motion errors calculated using the estimated rail show good agreement with the assumed values, and it is shown that the algorithm is effective in acquiring the corrective machining information to improve the accuracy of hydrostatic tables.

Keywords : Hydrostatic table, Corrective machining algorithm, Transfer function, Motion error analysis, Reverse analysis

1. Introduction

The finishing process to get the target accuracy of the ultra precision feed tables such as the aerostatic and hydrostatic tables depends entirely on the know-how of the skilled workers. For the theoretical systematization of this process, the authors have proposed the Transfer Function Method (TFM) which can analyze the linear and angular motion error by using the measured profile of the rail, the design variables and a transfer function[1]. The validity of the method also has been verified both theoretically and experimentally[2].

By applying this method, the motion errors of a hydrostatic table can be predicted directly from the measured rail profile, and using the relationship between the spatial frequency components of the rail profile and the motion errors, the corrective machining information for improving the motion accuracy can be easily obtained. But, this method has a limitation in practical applications because measuring the rail profile is not easy in many cases.

On the other hand, the motion errors represent the successive variations of the attitude of a table which are decided by the variables such as the rail profile, film force in the pads and the geometric relationship between the pads. Therefore, the relative relationship between the table and the rail is included in the motion errors. By estimating the rail profile from the motion errors by using the relationship, the corrective machining information can be obtained without the information on the rail profile. Especially, in the case of a double-side table, by using the relationship that the motion errors

☞ Manuscript received: January 17, 2004 ;
Accepted: March 10, 2004
Corresponding Author:
Email: pch657@kimm.re.kr
Tel: +82-42-868-7117, Fax: +82-42-868-7180

depend on the difference of the profile between the two rails, the corrective machining information can be obtained without the entire information on both rails.

In this paper, a corrective machining algorithm is proposed for improving the motion accuracy of the hydrostatic tables. The algorithm consists of three main processes. In the algorithm the reverse analysis is performed firstly to estimate the rail profile from the measured linear and angular motion errors. For the next step, the corrective machining information is obtained based upon the estimated rail profile. Finally, the motion errors on the correctively machined rail are analyzed by using the motion error analysis method[1,2]. These processes can be iterated until the analyzed motion errors are within the target accuracy. In order to verify the validity of the algorithm theoretically, the motion errors obtained by the estimated rail after the corrective machining, are compared with those obtained by the true rail assumed as the measured value.

2. Corrective Machining Algorithm

Fig. 1 shows the conceptual diagram of the corrective machining algorithm. Firstly, the variations of the film force are calculated using the measured motion errors and the geometric relationship between the pads of a hydrostatic table. Then the profile of the rail is estimated using the calculated variations of the film force and the transfer function. This algorithm is named as the Reverse Analysis Method (RAM) because the procedure is the reverse of the motion error analysis. In order to build the corrective machining information, machined positions and its amounts are assumed on the basis of the estimated rail profile, and the motion errors after the corrective machining are simulated using the previously proposed TFM. This procedure is performed iteratively until the simulated motion errors are within the target accuracy. After building the corrective machining information, practical machining is performed. In practical machining, since it is difficult to machine the rail exactly following the simulated machining information, there are differences between the simulated results and the pratically corrected results. In this case, the procedure is iteratively performed until the target accuracy is obtained.

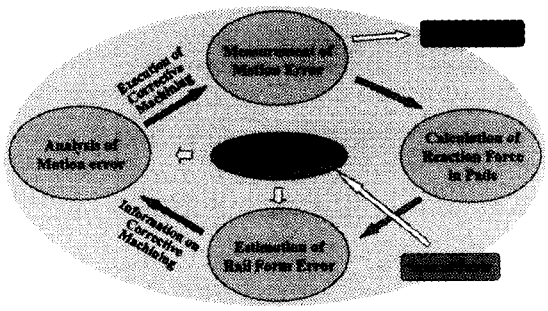

Fig. 1 Diagram of corrective machining alogorithm

3. Reverse Analysis Method

As mentioned above, the estimation algorithm for the rail profile is the reverse procedure of the motion error analysis. On the other hand, the previously explained analysis procedure is based on a single-side table. In the case of a double-side table, it is converted to an equivalent single-side table, if we treat the difference of both rail profiles as the rail profile of a single-side table. Then the rail profile can be estimated using the same procedure with a single-side table.

3.1 Modelling of a hydrostatic table

Fig. 2 shows the static equilibrium model of a hydrostatic table. By supposing that the film stiffness of a pad is constant within the range of displacement in the vertical direction, Eqs. (1) and (2) can be obtained from the equilibrium conditions of force and moment.

$$\sum_{i=1}^{m}\{f_{ei}(x)-K_0 z_i(x)\}=0 \tag{1}$$

$$\sum_{i=1}^{m}\{f_{ei}(x)-K_0 z_i(x)\}\left(X_{ci}+\frac{ml}{2}\right)=0 \tag{2}$$

$$x=\frac{ml}{2},\cdots,L-\frac{ml}{2}$$

where, m is the number of pads in a table, X_{ci} is the

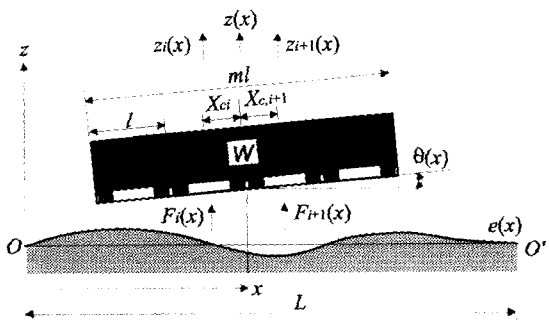

Fig. 2 The static equilibrium state of force in a single-side table

distance from the center of a table to the center of each pad, L is the length of the rail, l is the length of a pad, $F_i(x)$ and $z_i(x)$ are the film force and vertical displacement of ith pad, respectively, when the coordinate of the table center is x, and $\theta(x)$ is the inclined angle of the table. Also, $f_{ei}(x)$ is the variation of the film force corresponding to the rail form error $e(x)$ and K_0 is the film stiffness of a pad.

3.2 Transfer function

The transfer function is defined as the variation of the film force in a pad corresponding to the magnitude of the spatial frequency component of the rail form error as shown in Eq. (3). The validity of the definition, calculation method, and the characteristics of the transfer function have been clarified[1].

$$K(\omega) = \frac{f_e(\omega)}{e(\omega)} \tag{3}$$

3.3 Calculation of film force

When the motion errors are already known but the variation of the film force remains unknown, Eqs. (1) and (2) become a set of simultaneous equations with m unknown variables. Therefore it is impossible to obtain the nominial solution if the number of the pads exceeds 2. In order to solve the equations, another relationship which can decrease the number of the pads or increase the number of equations must be introduced. For introducing the new relationship, a relationship between the position of the table and the film forces of the pads are shown in Fig. 3. Considering the film force referred to the rail position, each pad that has the same dimension and has a different geometric relationship locates superposedly in the same position on the rail with increasing order. Using this superposed relationship, the number of unknown film forces can be decreased.

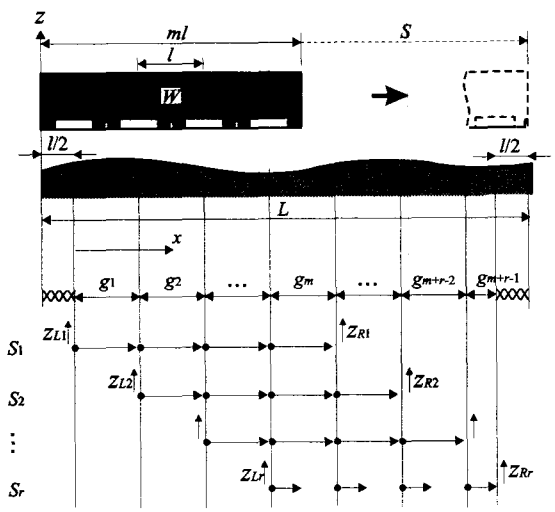

Fig. 3 Relationship between film force and the rail profile

Now, we divide the entire stroke of the table by the length of a pad, and call each of the divided sub-stroke as a period S_i, where i=1, ..., r. Then, if the number of film forces, $f_{ei}(x)$, in a period is m, the total number of the film forces become $m \times r$. On the other hand, we divide the rail length by the length of a pad, and call each of the divided length as a section. Defining $g_k(x)$ as the corresponding film force to each section, the number of the film forces referred to the rail position decreases to $k=m+r-1$, and the relationship between $g_k(x)$ and the film force $f_{ei}(x)$ corresponding to each period can be represented as Eq. (4).

$$f_{ei}(x) = g_k(x + X_{ci}) \qquad i = 1, \cdots, m, \quad j = 1, \cdots, r, \quad k = i + j - 1, \tag{4}$$

From Eqs. (1), (2) and (4), the relationship between the film forces and the motion errors in the period S_1 and S_2 is obtained as Eq. (5), where $z_{Lj}(x)$ and $z_{Rj}(x)$ are vertical displacements at the left-end and right-end of the table, respectively, which can be calculated from the linear and angular motion error.

$$\begin{aligned} &[u]\{g_{S1}\} = K_0 m(m^2-1)\begin{Bmatrix} z_{L1}(x) \\ z_{R1}(x) \end{Bmatrix} \\ &[u]\{g_{S2}\} = K_0 m(m^2-1)\begin{Bmatrix} z_{L2}(x) \\ z_{R2}(x) \end{Bmatrix} \\ &[u] = \begin{bmatrix} u_{11} & \cdots & u_{1m} \\ u_{21} & \cdots & u_{2m} \end{bmatrix}, \quad \begin{matrix} u_{1i} = 4m^2 + 3m - 1 - 6mi \\ u_{2i} = 6mi - 2m^2 - 3m - 1 \end{matrix} \\ &\{g_{S1}\}^T = \{g_1(x), \cdots, g_m(x)\}, \ \{g_{S2}\}^T = \{g_2(x), \cdots, g_{m+1}(x)\} \end{aligned} \tag{5}$$

Eq. (6) is the composed result of the two matrices in Eq. (5).

$$[u_{S12}]\{g_{S12}\} = K_0 m(m^2-1)\{z_{S12}\} \tag{6}$$

$$[u_{S12}] = \begin{bmatrix} u_{11} & u_{12} & \cdots & u_{1m} & 0 \\ u_{21} & u_{22} & \cdots & u_{2m} & 0 \\ 0 & u_{11} & \cdots & u_{1m-1} & u_{1m} \\ 0 & u_{21} & \cdots & u_{2m-1} & u_{2m} \end{bmatrix}$$

$$\{g_{S12}\}^T = \{g_1(x), \cdots, g_{m+1}(x)\},$$
$$\{z_{S12}\}^T = \{z_{L1}(x), z_{R1}(x), z_{L2}(x), z_{R2}(x)\}$$

Comparing Eq. (6) with Eq. (5), two more equations are added, but the number of the film forces is only increased by one. Extending this relationship up to the period S_r, the matrix equation for the all periods can be obtained as Eq. (7).

$$[U]\{G\} = K_0 m(m^2-1)\{Z\} \tag{7}$$

$$[U] = \begin{bmatrix} u_{11} & u_{12} & \cdots & u_{1m} & 0 & \cdots & 0 \\ u_{21} & u_{22} & \cdots & u_{2m} & 0 & \cdots & 0 \\ 0 & u_{11} & \cdots & u_{1\,m-1} & u_{1m} & \cdots & 0 \\ 0 & u_{21} & \cdots & u_{2\,m-1} & u_{2m} & \cdots & 0 \\ \vdots & & & \vdots & & & \vdots \\ 0 & \cdots & \cdots & u_{1\,m-r+1} & u_{1\,m-r+2} & \cdots & u_{1m} \\ 0 & \cdots & \cdots & u_{2\,m-r+1} & u_{2\,m-r+2} & \cdots & u_{2m} \end{bmatrix}$$

$$\{G\}^T = \{g_1(x), \cdots, g_m(x), \cdots, g_{m+r-1}(x)\}$$
$$\{Z\}^T = \{z_{L1}(x), z_{R1}(x), z_{L2}(x), z_{R2}(x), \cdots, z_{Lr}(x), z_{Rr}(x)\}$$

As the matrix $[U]$ has a size of $2r \times (m+r-1)$, it becomes a square matrix when r equals $m-1$. This means that if the moving stroke of the table exceeds the length of $(m-1)l$, the exact solution on the film forces can be obtained from the measured motion errors using Eq. (7).

On the other hand, using Eq. (8), the calculated film force $g_k(x)$ from Eq. (7) can be converted to $f_e(x)$, which is the film force when a pad moves successively on the rail.

$$f_e(x) = g_k(x), \quad \left\{\frac{1}{2}+(k-1)\right\}l \le x < \left\{\frac{1}{2}+k\right\}l \tag{8}$$
$$k = 1, \cdots, m+r-1$$

3.4 Estimation of the rail form error

The magnitude of spatial frequencies which is involved in the rail form error can be obtained by using the calculated film force and a transfer function in Eq. (3), and the rail form error can be obtained by superposing the profiles of the spatial frequencies. But considering the actual motion of the table shown in Fig. 3, since the table can not exceed the left-end and right-end of the rail, the motion errors corresponding to the half length of a pad at both ends of the rail cannot be obtained exactly.

In order to solve this problem, we define the obtainable range of the film force as the effective rail length L_f, and estimate the rail form error under the assumption that the film force is periodic within the effective rail length. It means that it is impossible to obtain the true rail form error. But in the view of the motion errors, the calculated film force includes the entire information on the motion errors. Therefore, even if the rail form error is calculated under the assumption of an arbitrary profile for the half length of a pad at both rail ends, the motion errors calculated from the rail form error are the same as the motion errors. Consequently, the estimated rail form error obtained by the RAM is not the same as that of the true rail, but the corrective machining information acquired from the estimated rail form error is sufficient to reduce the motion errors.

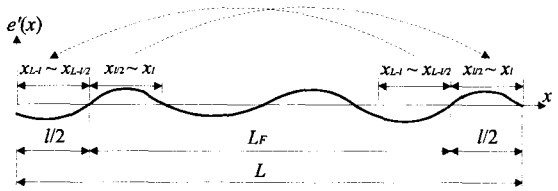

Fig. 4 Estimated periodic profile of rail

Now, ω_f is defined as a spatial frequency which has the same wave length as the effective rail length. Then, the magnitude of frequency components $e(\omega_f)$, which consists of the rail form error within the range of an effective rail length, can be calculated using the transfer function as in Eq. (9), and an estimated rail form error $e'(x)$ is represented in Eq. (10).

$$e(\omega_f) = f_e(\omega_f)/K(\omega_f) \tag{9}$$

$$e'(x) = \sum_{k=1}^{p/2}\left\{a_k \cos\frac{2k\pi}{L_f}\left(x-\frac{l}{2}\right) + b_k \sin\frac{2k\pi}{L_f}\left(x-\frac{l}{2}\right)\right\} + \frac{a_0}{2}, \quad x = 0, \cdots, L \tag{10}$$

In the case of the insensitive frequencies and relative high frequencies, the magnitudes of the transfer function are approximated to 0. Therefore, the rail form error components corresponding to the frequencies are overestimated by the round-off error calculated by Eq.(9).

On the other hand, generally there is no high frequency in the rail form error because the rail is processed by grinding. Even if there exist some high frequencies, their influence on the motion errors is negligible. The influence of the insensitive frequencies on the motion errors are also very small. Therefore, whether the rail form of the high frequency and

insensitive frequency components is included in the estimated rail form error or not, the motion errors by those have little difference.

In oder to utilize the above mentioned characteristics, the cut-off value on the magnitude of the transfer function is introduced in this algorithm. The frequency components at which the magnitude of the transfer function is smaller than the cut-off value, are ignored in the estimating process of the rail form error.

4. Building the Corrective Machining Information

There are many ways to remachine the rail form error. As one of them, the hand lapping process, which cuts the jutting parts of the rail straight with a constant width, is assumed as the remachining process in this research. An estimated rail form is remachined virtually step by step with the constant height, and the motion errors on the virtually machined rail is simulated in each step. If the simulated motion errors are within the target accuracy in each step, the simulation is finished and the accumulated datum on the preceded steps becomes the corrective machining information.

In the case of a double-pad table, any one of the two rails is initially selected as the reference rail. Then, the remachining information is calculated by assuming that the difference of the profile between the rails is the rail form error of the equivalent single-pad table. Finally, the corrective remachining is performed against the selected reference rail. Consequently, as the motion errors are further reduced, form errors of both rails become symmetrical.

5. Theoretical Verification of the Corrective Machining Algorithm

5.1 Verification method

For the theoretical verification, firstly, a rail form error $e(x)$ is assumed, and film force $f_e(x)$, linear motion error $z(x)$ and angular motion error $\theta(x)$ are calculated regarding the rail using the motion error analysis method. Then, the analyzed motion errors are assumed as the measured motion errors, and film force $f_e'(x)$ and rail form error $e'(x)$ is estimated by RAM. Initial values of $e(x)$ and $f_e(x)$ are compared with the estimated values of $f_e'(x)$ and $e'(x)$ in order to discuss the characteristics of the RAM. Also, motion errors $z'(x)$ and $\theta'(x)$ are calculated on the estimated rail $e'(x)$ and compared with the assumed motion errors $z(x)$ and $\theta(x)$.

For the next step, the corrective machining information $e_i(x)$ is calculated using the estimated rail form error $e'(x)$. Then, the correctively remachined rail forms $e_c(x)$ and $e_c'(x)$ can be calculated as shown in Eq. (11).

$$e_c(x) = e(x) - e_i(x), \quad e_c'(x) = e'(x) - e_i(x) \tag{11}$$

Finally, the motion errors $z_c(x)$, $\theta_c(x)$ on the remachined assumed rail $e_c(x)$ and the motion errors $z_c'(x)$, $\theta_c'(x)$ on the remachined estimated rail $e_c'(x)$ are calculated and compared for the verification of the entire algorithm.

The design variables of the rail and the table assumed for the theoretical verification are as shown in Table 1. The calculated transfer functions on the assumed design variables are also shown in Fig. 5. In the figure, ω_f is the spatial frequency on the basis of the effective rail length and ω_R is the spatial frequency on the basis of the entire rail length. In the case of pocket ratio $\beta = 0.8$, the components of ω/ω_f = 4, 10, 16, 22 become the insensitive frequencies as their magnitudes are

Table 1 Design variables used in the analysis

Rail length	L	600 mm
Number of pad	m	3
Table length	ml	300 mm
Table width	l_y	100 mm
Bearing clearance	h_0	52, 67 μm
Pocket width ratio	β	0.6, 0.8
Weight applied to table	W	300 N
Feeding parameter	ξ	1.0

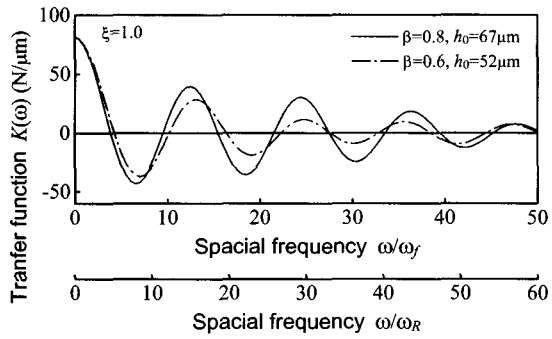

Fig. 5 Transfer function of assumed feed table

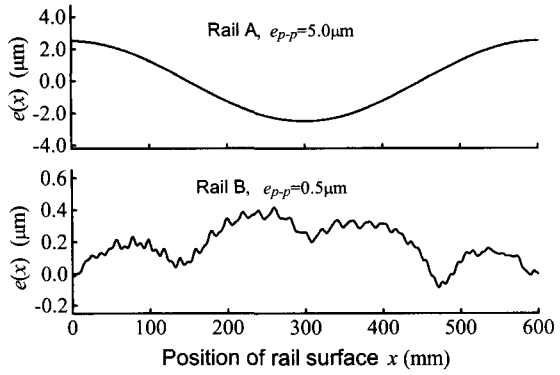

Fig. 6 Assumed rail profiles for simulation

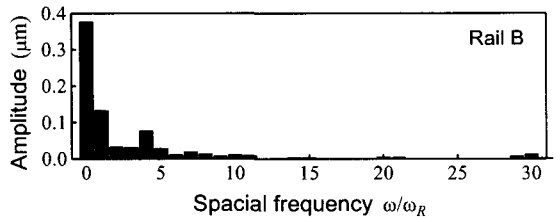

Fig. 7 Frequency components of rail B

approximated to 0. The assumed rail forms A and B are shown in Fig. 6. Rail A consists of only one component $\omega/\omega_f = 1$, and rail B consists of several components from $\omega/\omega_f = 1$ to 30. The magnitude of each component is shown in Fig. 7.

On the other hand, motion errors on the assumed rail A and B are calculated and assumed as the measured motion errors. They are shown in Fig. 11 and Fig. 13 when the motion errors obtained by the estimated rail form errors are compared with the initial motion errors.

5.2 Discussion on the film force calculation

Film force $f_e(x)$ obtained using the TFM is compared with $f_e'(x)$ which is calculated using the RAM on the assumed rail A and rail B as shown in Fig. 8. As both results show exact agreement, it is confirmed that the exact solution can be obtained by Eq. (4) in the case of the firm force.

5.3 Discussion on the estimation of rail

The estimated result on the rail A is shown in Fig. 9. Here, n_f is the maximum frequency to be calculated, and hereinafter, the spatial frequency is represented on the basis of the effective rail length L_f.

In the case of $n_f = 30$, the estimated rail profile has

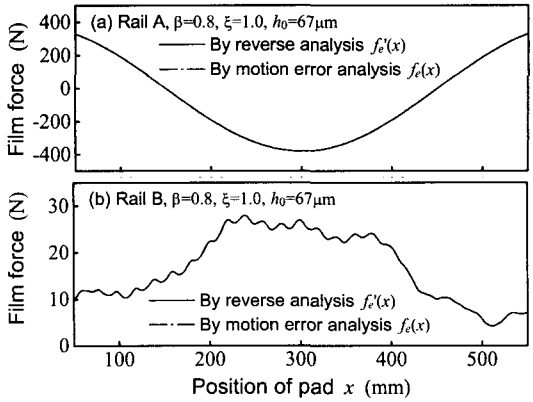

Fig. 8 Comparison of calculated forces exerted by rail form errors

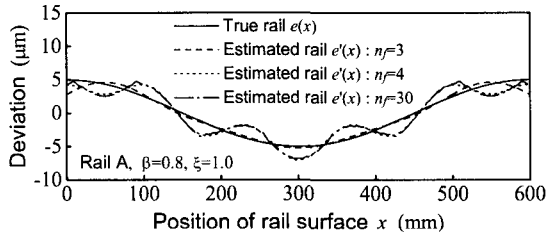

Fig. 9 Relationship between cut-off frequency and estimated rail

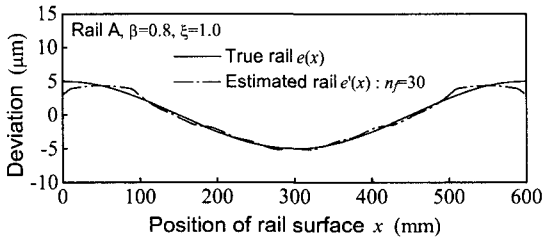

Fig. 10 Estimated profile by disregarding the insensitive frequencies and high frequencies

the components of $\omega/\omega_f = 1$ and 4. The aspect is the same when $n_f = 4$. It is because the component $\omega/\omega_f = 4$, which is the insensitive frequency as shown in Fig. 5, is overestimated in the process of the RAM. The motion errors may be reduced by the newly calculated corrective machining information on the basis of this estimated result. But, in this case, too much machining is needed by the overestimated frequency components.

On the other hand, in the case of $n_f = 3$, the estimated rail profile agrees well with the true rail(assumed rail) within the range of the effective rail length. Therefore, ignoring the frequency which is higher

than the minimum insensitive frequency, the estimated rail profile can be approximated to the true rail profile. But, in this case, there is a possibility that the effective high frequencies may be eliminated together.

In order to cover this disadvantage, the maximum magnitude of the transfer functions at the insensitive frequencies is treated as the cut-off value. The estimated result obtained by considering the cut-off value is shown in Fig. 10. In spite of extending to $n_f = 30$, the result agrees well with the true rail profile.

The motion errors analyzed using the true rail profile and the estimated rail profile are compared in Fig. 11. The two motion errors show good agreement, and the small difference, mainly shown in the linear motion error, is caused by the ignored frequency components. Also, though the rail profiles of both ends with the half size of a pad are assumed as arbitrary profiles, there exists no difference in the motion errors profiles.

The true and estimated rail profiles of the rail B are compared in Fig. 12. Both profiles are well matched with small deviations due to the ignored frequency components. The motion errors analyzed using the true and estimated rail profiles are compared in Fig. 13. It is also confirmed that there are little differences in motion errors.

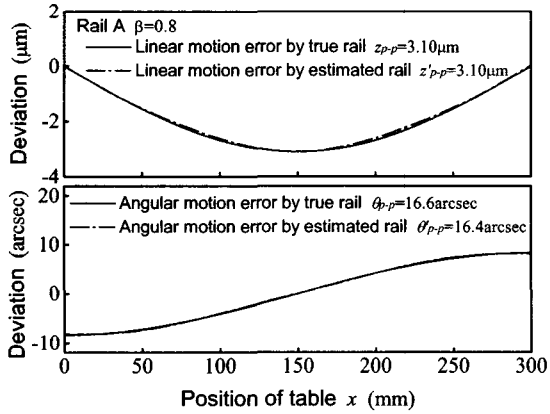

Fig. 11 Comparison of motion error by estimated rail with motion error by true rail in rail A

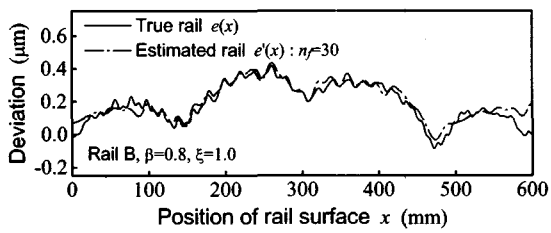

Fig. 12 Comparison of estimated rail with true rail in rail B

5.4 Discussion on the corrective machining

Firstly, it is assumed that the estimated rail profile is converted to the machining information, as it is. It means that the expected rail form error after the machining is zero. Therefore the motion errors by the rail are also expected to be zero. Profile of the true rail after the corrective machining using the estimated rail profile in rail B is shown in Fig. 14(a) by the solid line. The profile

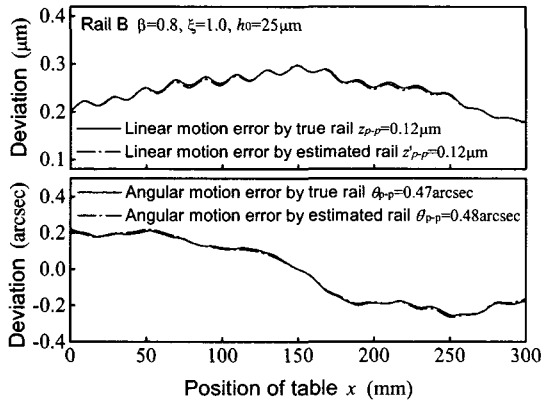

Fig. 13 Comparison of motion error by estimated rail with motion error by true rail in rail B

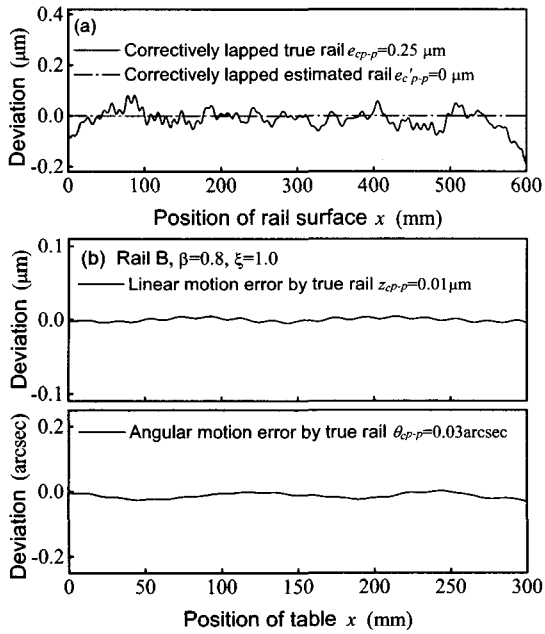

Fig. 14 Variation of rail profile and motion errors after completely removing estimated profile

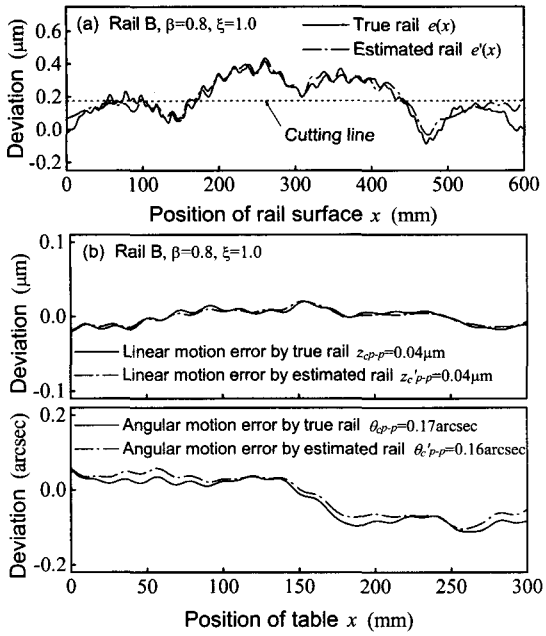

Fig. 15 Variation of motion errors after partly removing estimated profile

is caused by the difference between the true rail and the estimated rail. Fig. 14(b) shows the simulated motion errors on the correctively machined true rail profile of Fig. 14(a). The motion errors do not go to perfectly zero because of the ignored frequency components. But the amount of error is small enough and decreases to one tenth of the initial errors shown in Fig. 13.

Secondly, aspects are shown in Fig. 15 when the estimated rail profile is partly corrected. Plain cutting is assumed as shown in Fig. 15(a) by the dotted line. Motion errors obtained by the true rail and the estimated rail after the corrective machining are shown in Fig. 15(b). Both errors show good agreement.

From the above simulated results, it is confirmed that the proposed corrective machining algorithm is very effective in improving the motion errors of hydrostatic bearing tables.

6. Conclusions

The results obtained in this work are as follows;

1) Modelling method for estimating the film force using the measured motion errors is proposed. From the calculated results, it is confirmed that the exact solution on the film force can be obtained by the method if the stroke of the table exceeds the length of $(m-1)l$.
2) In the case of estimating the rail profile using the calculated film force, the estimated rail profile is slightly different from the true rail profile due to the ignored insensitive frequency and high frequency components. But, the motion errors calculated using both rail profiles show good agreement. From this result, it is confirmed that the Reverse Analysis Method is effective in the corrective machining process.
3) Even in the case where the estimated rail profile is partly corrected, the motion errors obtained by the estimated rail profile show good agreement with those obtained by the true rail. Therefore, it is possible to build the corrective machining information corresponding to the target accuracy.

From these results, the validity of the corrective machining algorithm is theoretically verified, and a study on the experimental verification of the algorithm is going to be performed in the near future.

Acknowledgement

The authors gratefully acknowledge the support of Ministry of Science and Technology under the National Research Laboratory project.

References

1. Park, C. H., Oh, Y. J., Lee, C. H. and Hong, J. H., "Theoretical Verification on the Motion Error Analysis Method of Hydrostatic Bearing Tables Using a Transfer Function," Int. J. of KSPE, Vol. 4, No. 2, pp. 64-70, 2003.
2. Park, C. H., Oh, Y. J., Lee, C. H. and Hong, J. H., "Experimental Verification on the Motion Error Analysis Method of Hydrostatic Bearing Tables Using a Transfer Function," Int. J. of KSPE, Vol. 4, No. 2, pp. 57-63, 2003.
3. Kodama, S. and Suda, N., "Matrix Theory for the System Control," The Society of Instruments and Control Engineers (Japan), 2nd Edition, 1981.